RSC Advances

PAPER

View Article Online
View Journal | View Issue

Cite this: *RSC Adv.*, 2016, **6**, 78684

Versatile interactions of boron fullerene B_{80} with gas molecules†

Guilherme Colherinhas,[a] Eudes Eterno Fileti*[b] and Vitaly V. Chaban[b]

Received 17th June 2016
Accepted 14th August 2016

DOI: 10.1039/c6ra15793a

www.rsc.org/advances

Stable all-boron fullerene B_{80} supplements a family of elemental cage molecules. These molecules may initiate a drastic rise to intriguing new chemistry. The principal stability of B_{80} was recently demonstrated using photoelectron spectroscopy. We report the systematic investigation of different aspects of B_{80} interactions with small gas molecules—such as carbon dioxide, molecular hydrogen, hydrogen sulfide, hydrogen fluoride, ammonia and sulfur dioxide—employing density functional theory. We found peculiar interactions between B_{80} and ammonia resulting in the formation of a weak boron–nitrogen covalent bond in one of their local-minimum configurations. Hydrogen fluoride maintains a weak hydrogen bond with B_{80}. The boron fullerene was found to be strongly polarizable, with its electron density distribution changing significantly even in the presence of low-polar gases. The binding energies of the gas molecules to B_{80} are generally in direct proportion to their dipole moments. Valence bands are predominantly localized on B_{80}. According to the present findings, one of the prospective applications of B_{80} in future may be gas capture and separation.

Introduction

Boron is a second-period element possessing five electrons. In spite of being located next to carbon, boron chemistry has been investigated to a much lesser extent, as compared to that of carbon, thus far. The known structures of elemental boron include an icosahedral B_{12} motif connected in an ordered manner, *e.g.* like in α-rhombohedral boron. The dangling bonds in B_{12} can be saturated with hydrogen atoms giving rise to boranes. In turn, stable all-boron clusters are different. For instance, the symmetry of B_{12} is C_{3v} (symmetric planar structure). Such clusters can contain up to 36 atoms, while retaining their planar and quasi-planar shapes. Zhai and coworkers[1] recently reported B_{40} cluster, which was produced in a laser-vaporization supersonic source. The detection was performed by means of photoelectron spectroscopy in the gas phase. The authors also carried out quantum-chemical calculations, which revealed that the newly obtained cluster adopts a variety of structures, such as a planar anion (C_s symmetry) and a neutral all-boron cage (D_{2d} symmetry). The B_{40} cluster is not perfectly smooth exhibiting 8 quasi-planar triangles B_6, 2 hexagonal holes, and 4 heptagonal holes.[1] The observation published by Zhai and coworkers marks a milestone in the boron chemistry. A few months later, Chen and coworkers[2] obtained an axially chiral borospherene B_{39}^- detected by photoelectron spectroscopy and deciphered by electronic-structure calculations and the global minimum search procedure. Theoretical analysis showed that B_{39}^- possesses a C_3 cage global minimum with a close-lying cage isomer. Both cages are chiral with degenerate enantiomers.[2]

Stable all-boron fullerenes supplement a family of elemental single-element molecules.[3–12] These molecules may initiate a drastic rise of intriguing new chemistry, which is not reminiscent of the carbonaceous nanoscale compounds. Furthermore, these new molecules can become efficient building blocks and inorganic ligands to foster bottom-up construction of hybrid nanostructures combining desirable physical chemical properties and eliminating undesirable ones. Exohedral derivatives and encapsulation of metal atoms/ions constitutes a particularly interesting goal.[13,14] It must be, however, noted that macroscopic synthesis and isolation of the all-boron fullerene still remains a challenge for the community.

Computer simulations based on the density functional theory (DFT) or higher-level *ab initio* methods play an important role in predicting structure, stability, properties, and potential energy surfaces of the all-boron molecules.[15–25] Garcia and coworkers[23] performed a profound DFT study of the binding and solvation of B_{80} in the cholinium-based ionic liquids (ILs). After geometry optimization, a chemical bond was identified between the carboxyl group of the anion and the boron atom of B_{80}. This important result suggests that the carboxyl containing ILs constitute suitable solvents for B_{80}. Furthermore, ions with aromatic motifs could be good solvents for B_{80} as well, since

[a]*Departamento de Física-CEPAE, Universidade Federal de Goiás, 74690-900, Goiânia, Brazil. E-mail: gcolherinhas@gmail.com*

[b]*Instituto de Ciência e Tecnologia, Universidade Federal de São Paulo, 12231-280, São José dos Campos, SP, Brazil. E-mail: fileti@gmail.com; vvchaban@gmail.com*

† Electronic supplementary information (ESI) available: Tables S1–S4 summarize raw computation data to facilitate reproduction of the reported results. See DOI: 10.1039/c6ra15793a

strong interactions emerge due to π-stacking. The boron atoms act as hydrogen bond acceptors engendering hydrogen bonds with the nonaromatic cholinium cation.

Wang considered a different conformation of B_{80}, a volleyball-shaped one comprising 12 pentagonal pyramids, 8 hexagonal pyramids, and 12 hollow hexagons.[16] DFT was employed to characterize structure and electronic stabilities. Thanks to the improved aromaticity associated with the distinct configuration, the volleyball-shaped B_{80} appears significantly more stable, as compared to the previously proposed boron buckyball. Cheng applied high-level *ab initio* calculations and argued that not all small all-boron clusters are planar and quasi-planar using B_{14} as an example.[25] B_{14} was shown to exhibit a global minimum corresponding to a flat cage with a closed-shell electronic structure and strong aromaticity. The band gap of this structure is notably large, 2.69 eV.

Lv and coworkers[26] predicted stability of the B_{38} fullerene analogue by means of swarm structure searching calculations based on the first principles. The obtained structure exhibits high symmetry consisting of 56 triangles and 4 hexagons providing an optimal void at the center of the cage. This structure was found to be more energetically stable, as compared to planar and tubular ones. A large band gap, 2.25 eV, and strong aromaticity were derived for this local minimum. Olguin and coworkers[18] considered hydrogen storage using B_{80} and calcium atoms adsorbed on its surface. These authors showed that a single calcium atom prefers to occupy a hexagonal site rather than a pentagonal site, in contrast to what was reported before. Calculations of fixed number of calcium atoms (12, 20, 32) revealed a uniform coverage of B_{80}.

In the present work, we report DFT calculations of the physical properties of the $X@B_{80}$ complexes, where X is a gas molecule: H_2, CO_2, H_2S, HF, NH_3, SO_2. We considered geometric parameters, binding energies, dipole moments, localizations of molecular orbitals, partial charges, and electronic excitations. The B_{80} closed cage can be directly constructed from the B_{40} clusters. Thus, B_{80} is the most probable all-boron fullerene to be experimentally available in the near future. Having information on the nature and regularities of the all-boron fullerene interactions with small omnipresent molecules provides an opportunity to discuss its prospective applications.

Methodology

All properties of all systems were computed by pure density functional theory employing the well-established BLYP exchange-correlation functional.[27,28] The wave function was approximated by the atom-centered split-valence double-zeta polarized basis set, 6-31G(d). The non-valence (core) electrons were represented by the CEP potentials[29] to accelerate wave function convergence. The self-consistent field convergence criterion was set to 10^{-6} Hartree. On top of this, Grimme's empirical dispersion correction for the weak dispersion attraction[30] was supplemented at all stages of the computation using local modification "IOP(3/124 = 3)".

The binding energy was assessed as a difference between the total potential energy of the molecular complex and the energies of its counterparts. The basis set superposition error (BSSE) was identified using ghost atoms (the counterpoise approach). All reported binding energies do not include BSSE. Where mentioned, the geometry optimization was performed until the convergence criteria were met (12 kJ nm^{-1} for maximum force, 8 kJ nm^{-1} for root-mean-squared force, 0.18×10^{-3} nm for maximum displacement, and 0.12×10^{-3} nm for root-mean-squared displacement). The subsequent frequency analysis was used to exclude transition states from the binding energy computation. The potential energy surface was scanned by altering distance between the surface of B_{80} and the center-of-mass of gas molecule.

Electrostatic potential was approximated by a set of point charges following the CHELPG procedure.[31] Time-dependent DFT calculations were performed for the optimized complexes to derive absorption spectrum. The BLYP functional[27,28] and the larger basis set, atom-centered split-valence triple-zeta polarized, 6-311G(d,p), was used. Implementations of the referenced quantum-chemical methods in Gaussian 09 were employed.[32]

Results and discussion

The geometry of B_{80} was optimized in vacuum and in the presence of small gas molecules (Fig. 1). The investigated set of molecules (CO_2, H_2, H_2S, HF, NH_3, SO_2) includes both non-polar and polar gases (at normal conditions) with significantly different dipole moments. Interestingly, B_{80} somewhat changes bond lengths, ΔR, and bond angles of the gas molecules, the largest changes occurring in H_2S and NH_3: -76×10^{-3} Å and -133×10^{-3} Å, respectively. The largest alteration of the valence angle was found to take place in $NH_3@B_{80}$: from 106.87° (NH_3 in vacuum) to 108.15° (adsorbed NH_3). Some changes are also observed in the covalent boron–boron bond length of B_{80}. The maximum bond length increases by 0.056 Å and the minimum bond length decreases by 0.013 Å, when the gas molecules in adsorbed. Table S2† summarizes the effect of each gas molecule. Certain geometric changes suggest that quite a strong interaction of the gas molecules and B_{80} take place.

The closest-approach distances in the $X@B_{80}$ complexes are 3.15 Å for $X = CO_2$, 2.79 Å for $X = H_2$, 2.53 Å for $X = H_2S$, 2.56 Å for X = HF, 1.67 Å for $X = NH_3$, 3.00 Å for $X = SO_2$. The gas

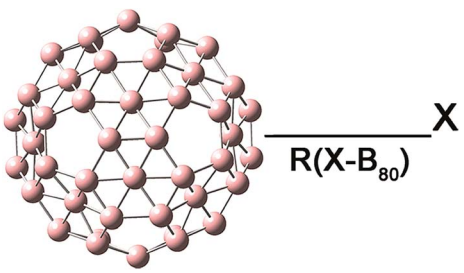

Fig. 1 The optimized ground state geometry of B_{80}. The scheme shows the calculations (rigid scan) of binding energies for gas molecules X: CO_2, H_2, H_2S, HF, NH_3, SO_2.

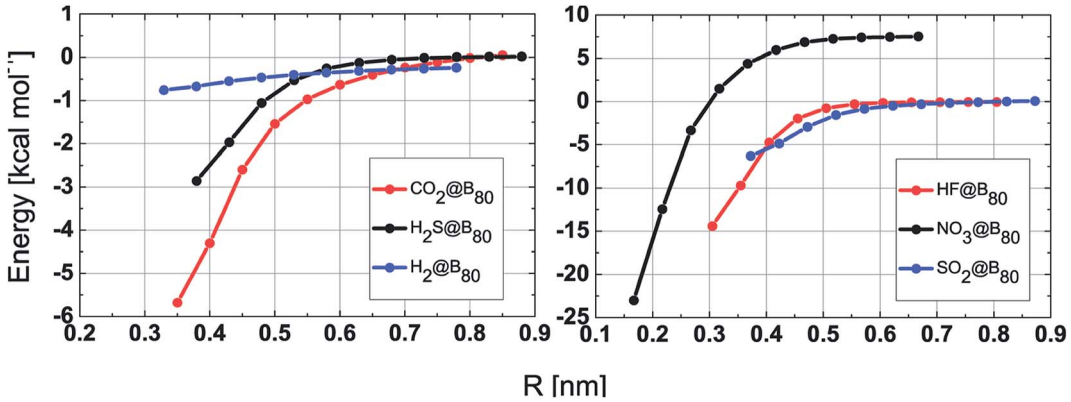

Fig. 2 Binding energy *versus* intermolecular distance, $R(X-B_{80})$, in the $X@B_{80}$ complexes. See legend for designation of gas molecules.

Table 1 Coefficients A and B obtained from fitting of the binding energy curves to $A \times R^{-6} + B \times R^{-1}$. No electrostatic interaction occurs between H_2 and B_{80}. Therefore, the corresponding curve (Fig. 2) was fitted to the $A \times R^{-6}$ form

Coefficient	$CO_2@B_{80}$	$H_2@B_{80}$	$H_2S@B_{80}$	$HF@B_{80}$	$NH_3@B_{80}$	$SO_2@B_{80}$
$A \times 10^3$ kcal mol^{-1} nm^{-6}	-9.78 ± 1.29	-0.20 ± 0.06	-8.93 ± 0.76	-11.7 ± 1.3	-0.70 ± 0.17	-17 ± 2
$B \times 10^3$ kcal mol^{-1} nm^{-1}	-343 ± 127	—	-45.9 ± 50	-348 ± 253	1120 ± 760	-276 ± 154

atoms, whose distance to the surface of B_{80} appeared smallest, are carbon in CO_2, hydrogen in H_2S, hydrogen in HF, nitrogen in NH_3, oxygen in SO_2. It contradicts intuition that hydrogen atoms are closer to B_{80} than the sulphur atom in H_2S, since sulphur is expected to have a larger partial charge (analogous to oxygen in water) and a higher van der Waals attraction constant. The corresponding binding energies B_{80}–gas are negative amounting to -5.679 ($X = CO_2$), -0.3548 ($X = H_2$), -2.856 ($X = H_2S$), -14.40 ($X = HF$), -22.99 ($X = NH_3$), -6.293 kcal mol^{-1} ($X = SO_2$). The binding energies are quite large, besides the cases of H_2 and H_2S, suggesting that B_{80} may offer an interesting gas capture behaviour. Furthermore, sufficiently different results for different gas molecules have practical implications for separation setups. For instance, -22.99 kcal mol^{-1} must be enough to separate NH_3 from gas mixtures since this binding energy is significantly larger than the kinetic energy of thermal motion of NH_3 (~0.6 kcal per mol per degree of freedom) at room temperature and below. Hydrogen fluoride also exhibits high affinity to B_{80}, -14.40 kcal mol^{-1}. This result deserves more comprehensive investigation in the context of HF removal upon oil rectification. Molecular hydrogen interacts with B_{80} very weakly, in accordance with theoretical expectations. Only weak London forces are present. Although CO_2 does not have a dipole moment, its binding to B_{80} is relatively strong, probably due to non-zero higher electric moments and electronic polarization of the boron fullerene. SO_2 provides similar energy, while coordinating B_{80} by both oxygen atoms. Carbon dioxide was recently computationally demonstrated to follow both chemisorptions and physisorption mechanisms on B_{80}.[21] According to the computations, formation of the chemisorbed

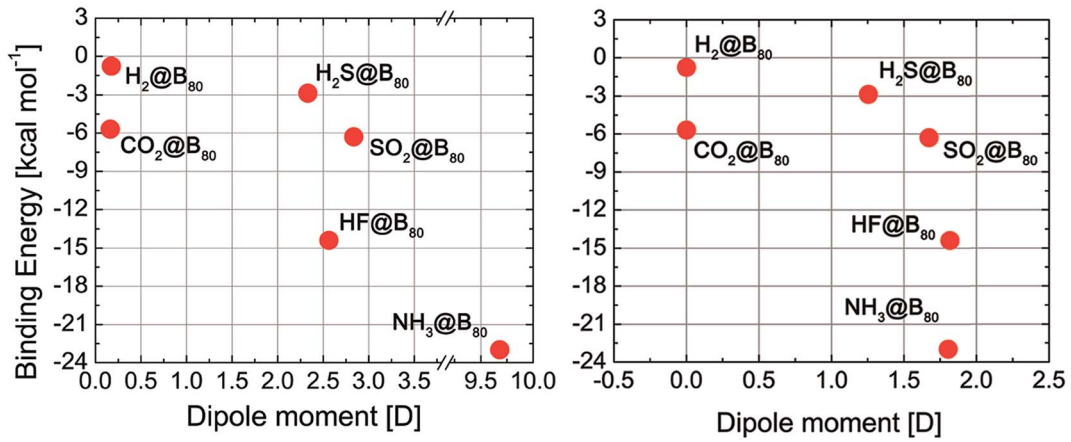

Fig. 3 (Left) Maximum binding energy, $E_{max}(X-B_{80})$, *versus* dipole moment of the $X@B_{80}$ complex. (Right) $E_{max}(X-B_{80})$ *versus* dipole moment of X.

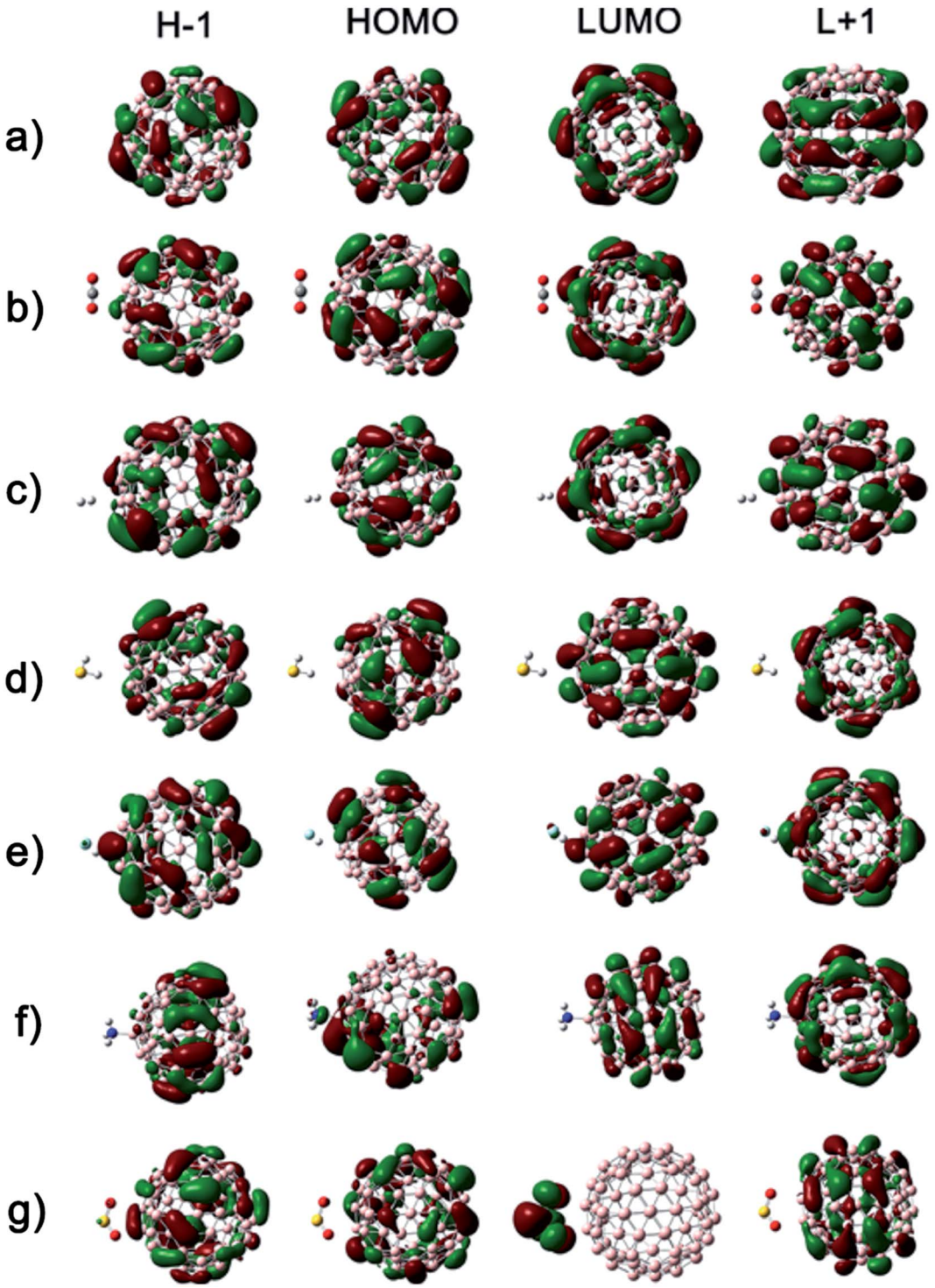

Fig. 4 Geometries and localizations of the most important molecular orbitals—highest occupied (HOMO), lowest unoccupied (LUMO), HOMO−1, and LUMO+1—in isolated B_{80} and X@B_{80} complexes. (a) B_{80}; (b) CO_2@B_{80}; (c) H_2@B_{80}; (d) H_2S@B_{80}; (e) HF@B_{80}; (f) NH_3@B_{80}; (g) SO_2@B_{80}. Boron atoms are pink, carbon atoms are grey, oxygen atoms are red, hydrogen atoms are white, sulphur atoms are yellow, fluorine atoms are cyan, nitrogen atoms are blue.

configurations is both thermodynamically and kinetically favourable. B_{80} can probably be used to separate CO_2 from its mixtures, such as CO_2/N_2, CO_2/CH_4 *etc.*, being important for the carbon capture technologies. In the present work, we only considered physisorption in the CO_2@B_{80} complex, whose energy appears in a good agreement with data of Sun and co-workers, 6–7 kcal mol^{-1} for different physisorption sites.[21] We did not find a binding energy in the case of SO_2, which would be comparable with that observed for CO_2. Sulfur dioxide is not a direct analogue of CO_2, *e.g.* the O–S–O angle is 119 degrees,

unlike the O–C–O angle, 180 degrees. A rigorous way to prove that would be to run a global minimum search, which is however very time-consuming for this size of the system.

Starting from the local-minimum molecular configuration, the B_{80}–X distance (Fig. 1) was increased stepwise, by 0.5 Å per step, to obtain a binding energy dependence on the intermolecular distance. The positive energies ($E \sim r^{-12}$) caused by electron–electron repulsion at small separations were not investigated due to the lack of interest to them in the context of the present study. In turn, the attraction part of the curve allows to understand physical nature of the B_{80}–gas interactions at the closest-approach distance and medium separations.

Remarkably, NH_3, which demonstrates the strongest binding to B_{80} in the local-minimum molecular configuration, starts repelling at 3.17 Å. Being in direct contact with B_{80}, NH_3 strongly polarizes its surface forming a weak polar covalent bond, N–B, based on the interatomic distance, 1.67 Å. As NH_3 is pulled away, the dipole moment vectors of both molecules reorient leading to domination of the repulsive electrostatic interactions. Note that we simulated a rigid potential energy scan. Therefore, only the selected interatomic distance changes, while all angles and dihedrals are kept fixed. If rotation of ammonia was allowed, we would not have observed repulsive energies on the potential energy curve. The derived energy curves were fitted to the $A \times R^{-6} + B \times R^{-1}$ form, in which A and B are empirical coefficients, R^{-6} approximates decay of the dispersion energy, R^{-1} approximates decay of the electrostatic energy as the distance increases.

Binding energy analysis reveals a general correlation between the dipole moment μ of the gas molecules: larger μ means larger E(X–B_{80}). Indeed, binding in NH_3@B_{80}, HF@B_{80}, and SO_2@B_{80} is stronger. This finding means that not only van der Waals interactions occur between the investigated molecules, but also the electrostatic term delivers a significant portion of the binding energy, as Table 1 suggests. Fig. S1 from ESI† presents results to support this conclusion. For this, we calculated the energy for two of the investigated complexes without the use of the dispersion correction. Whereas the dispersion correction is essential for the proper description of the interaction energy between the counterparts of the complex, the electrostatic component is significant and depends crucially on the dipole moment of the gas molecule.

Fig. 3 depicts dipole moments—both that of the gas molecule in vacuum and that of the X@B_{80} complexes—as a function of the maximum binding energy.

High dipole moments of NH_3 and HF are in line with their strong binding to B_{80}, −(14–23) kJ mol^{-1}. In turn, H_2 is attracted by B_{80} very weakly. CO_2 has $\mu = 0$ D, but interacts quite strongly due to partial electrostatic charges on the carbon atom and both oxygen atoms. Based on the binding energy, H–B distance (2.56 Å), and F–H–B angle (112.8°), HF engenders a weak hydrogen bond with B_{80}. The HF molecule is coordinated by one of the pentagons of B_{80}. The pentagons comprise electron rich boron atoms. The negatively charged boron atoms compete for the coordination of the electron poor hydrogen atom, q(H) = +0.305e. Due to adsorption, HF becomes charged, since q(F) = −0.474e.

HOMO and LUMO of the X@B_{80} complexes are primarily localized on B_{80} (Fig. 4 and Table S3†). However, in the strongly interacting complexes X@B_{80}, the influence of X on the valence and conduction bands is significant. Compare the HOMO energies in B_{80} (−5.0231 eV) to −5.2758 eV when X = H_2S, −5.2665 eV when X = HF, −4.6254 eV when X = NH_3, and −5.1003 eV when X = SO_2. The effects of X = CO_2 and X = H_2 are

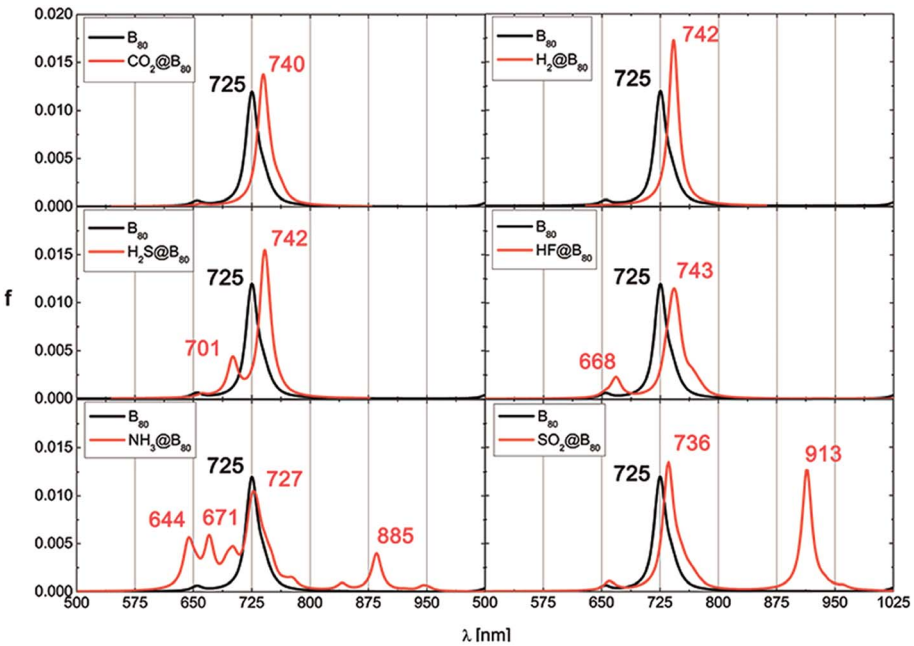

Fig. 5 Electronic transition spectra of the X@B_{80} complexes computed using TD-DFT. Analogous spectrum of isolated B_{80} is given for reference (black line). Lorentzian broadening with the half-height width of 16 was applied.

marginal, whereas both molecules have a zero dipole moment. The HOMO–LUMO band gaps exhibit a similar trend: 1.1148, 1.1024, 1.0539, 0.8204, and 0.5274 eV in B_{80}, $H_2S@B_{80}$, $HF@B_{80}$, $NH_3@B_{80}$, and $SO_2@B_{80}$, respectively. In $NH_3@B_{80}$, HOMO is shared by B_{80} and NH_3, whereas in $SO_2@B_{80}$, LUMO is localized on SO_2. These are the reasons of the significant differences of their band gaps from those in other $X@B_{80}$ complexes.

Electronic transitions in $X@B_{80}$ produce a single intense band at 700–750 nm (Fig. 5). Table S4† summarizes the orbital-by-orbital transitions for comprehensive analysis. All transitions with oscillator strength $>1 \times 10^{-3}$ are included. The major band originated from B_{80} (maximum at 725 nm) shifts somewhat to higher wavelengths, when $X = H_2$ and $X = CO_2$. In turn, other gas molecules produce signals at differing wave lengths (Fig. 5). The most significant changes are observed in the cases of $NH_3@B_{80}$ (new peaks at 644, 671, 727, 885 nm) and $SO_2@B_{80}$ (new peaks at 736, 913 nm). The peaks corresponding to electronic excitations are in concordance with stronger binding between B_{80} and gas molecules, as exemplified above.

Electron density distribution on different boron atoms of B_{80} is not equivalent (Fig. 6). Indeed, Zhai and coworkers underlines that the observed B_{40} cluster is not perfectly smooth containing quasi-planar triangles, hexagonal and heptagonal holes.[1] Following the CHELPG fitting of the electron density to reproduce dipole moments by means of the point charges

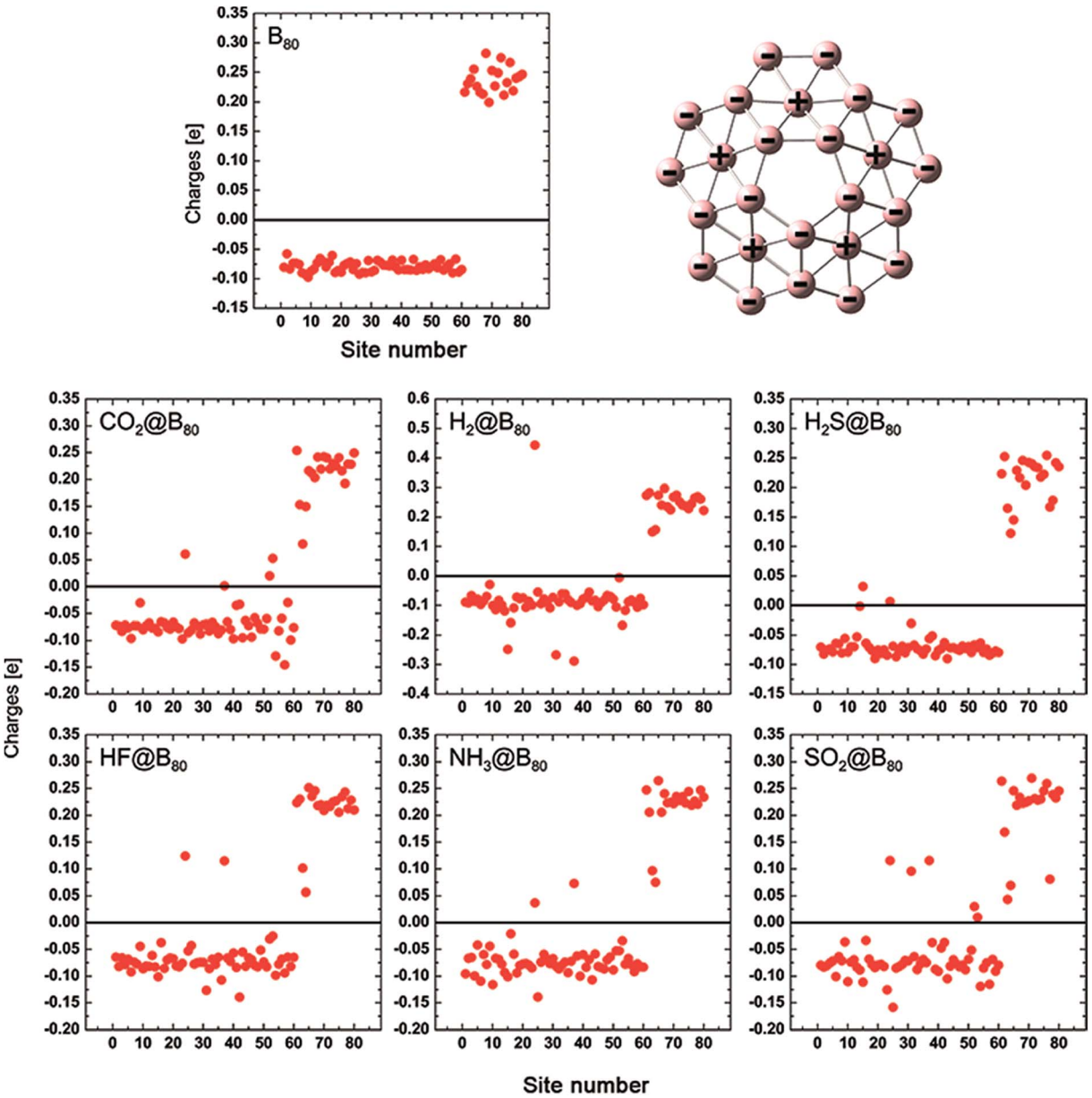

Fig. 6 Electrostatic CHELPG charges on each atom of B_{80} in the $X@B_{80}$ complexes. In the isolated boron fullerene, the boron atom at the center of the hexagon is electron deficient, whereas all the hexagon atoms are electron rich. The positively and negatively charged atoms are grouped together (top). Numbering is identical in all instances.

located on each atom, we revealed boron hexagons with all negative vertices compensated by one central electron deficient boron atom (Fig. 6). The charges of vertices range between −0.05 and −0.10e, while the charges of the central atoms range between +0.20 and +0.30e. The influence of all gas molecules, even nonpolar ones, can be observed. The largest perturbations of the charge distribution occur in the cases of X = HF, X = NH_3, and X = SO_2, *i.e.* gas molecules with higher dipole moments. Furthermore, this result presents an additional evidence of the large polarizability of the B_{80}, where the distribution of point charges within B_{80} depends substantially on the adsorbed gas molecule. The magnitude of the observed perturbation is generally proportional to the dipole moment of the respective gas molecule.

Conclusions

An electronic-structure-based investigation of the interactions of boron fullerene B_{80} with small gas molecules has been performed. Density functional theory was employed to obtain the wave functions and scan the potential energy surfaces. Binding energies, dipole moments of gases, band gaps, partial electronic charges, electronic transition spectra, energy levels of the valence of conduction bands, localization of orbitals, and selected geometric parameters characterizing gas adsorption on the external surface of B_{80} were analyzed. We found that binding energy generally correlates with the dipole moment of the gas molecule, being higher for more polar molecules and *vice versa*. Therefore, B_{80} was demonstrated to be a highly polarizable compound, whose response to the external electric field imposed by single molecules, is easily detectable. HOMO and LUMO are primarily localized on B_{80}. Electronic spectra of NH_3@B_{80} and SO_2@B_{80} are drastically different from those of the isolated boron fullerene. Fullerenes made out of carbon atoms do not capture gas molecules *via* chemisorption and hydrogen bonding, while we revealed that B_{80} does. Thus, B_{80} is more efficient for capturing certain gases, in particular CO_2, NH_3, and HF. Both nanostructures are highly polarizable due to their finite curvatures. Polar molecules induce local dipole moments on the fullerene surface and increase interaction energies.[33,34] The revealed electronic properties of B_{80} – such as systematically arranged electron deficient and electron rich atoms – suggest its less hydrophobic behaviour, as compared to carbonaceous fullerenes. Improved aqueous solubility of B_{80} may foster its practical application even further.

Two particularly interesting cases were identified. NH_3 forms a nonpolar covalent bond with B_{80} (−22.9 kcal mol^{-1}). HF forms a weak hydrogen-boron hydrogen bond (−14.4 kcal mol^{-1}). These findings supplement an important recent result of Sun and coworkers,[21] who hypothesized CO_2 chemisorption on B_{80}. As soon as B_{80} is synthesized and separated in macroscopic quantities, the information on peculiar binding will foster its practical applications. A non-intuitive ability of B_{80} to capture HF motivates to investigate its behaviour with other strongly polar molecules. The present work constitutes an important example of how computational chemistry can serve community before certain compounds are obtained in the macroscopic quantities to foster real experiments.

Acknowledgements

Support was obtained from FAPEG, CNPq, FAPESP, CAPES. The Neumann supercomputing cluster is hereby acknowledged.

References

1 H. J. Zhai, Y. F. Zhao, W. L. Li, Q. Chen, H. Bai, H. S. Hu, Z. A. Piazza, W. J. Tian, H. G. Lu, Y. B. Wu, Y. W. Mu, G. F. Wei, Z. P. Liu, J. Li, S. D. Li and L. S. Wang, *Nat. Chem.*, 2014, **6**, 727–731.
2 Q. Chen, W. L. Li, Y. F. Zhao, S. Y. Zhang, H. S. Hu, H. Bai, H. R. Li, W. J. Tian, H. G. Lu, H. J. Zhai, S. D. Li, J. Li and L. S. Wang, *ACS Nano*, 2015, **9**, 754–760.
3 P. A. Denis, C. Pereyra Huelmo and A. S. Martins, *J. Phys. Chem. C*, 2016, **120**, 7103–7112.
4 P. A. Denis and M. Yanney, *RSC Adv.*, 2016, **6**, 50978–50984.
5 A. Avramopoulos, N. Otero, P. Karamanis, C. Pouchan and M. G. Papadopoulos, *J. Phys. Chem. A*, 2016, **120**, 284–298.
6 T. B. Tai and M. T. Nguyen, *Phys. Chem. Chem. Phys.*, 2015, **17**, 13672–13679.
7 N. M. Tam, H. T. Pham, L. V. Duong, M. P. Pham-Ho and M. T. Nguyen, *Phys. Chem. Chem. Phys.*, 2015, **17**, 3000–3003.
8 G. Garcia, M. Atilhan and S. Aparicio, *J. Phys. Chem. B*, 2015, **119**, 10616–10629.
9 S. Polad and M. Ozay, *Phys. Chem. Chem. Phys.*, 2013, **15**, 19819–19824.
10 D. E. Bean, J. T. Muya, P. W. Fowler, M. T. Nguyen and A. Ceulemans, *Phys. Chem. Chem. Phys.*, 2011, **13**, 20855–20862.
11 R. Long, Y. Dai and B. Huang, *J. Phys. Chem. Lett.*, 2013, **4**, 2223–2229.
12 R. Zalesny, O. Loboda, K. Iliopoulos, G. Chatzikyriakos, S. Couris, G. Rotas, N. Tagmatarchis, A. Avramopoulos and M. G. Papadopoulos, *Phys. Chem. Chem. Phys.*, 2010, **12**, 373–381.
13 Q. L. Lu, Q. Q. Luo, Y. D. Li and S. G. Huang, *Phys. Chem. Chem. Phys.*, 2015, **17**, 20897–20902.
14 W. J. Tian, Q. Chen, H. R. Li, M. Yan, Y. W. Mu, H. G. Lu, H. J. Zhai and S. D. Li, *Phys. Chem. Chem. Phys.*, 2016, **18**, 9922–9926.
15 H. Y. He, R. Pandey, I. Boustani and S. P. Karna, *J. Phys. Chem. C*, 2010, **114**, 4149–4152.
16 X. Q. Wang, *Phys. Rev. B: Condens. Matter Mater. Phys.*, 2010, **82**, 153409.
17 J. T. Muya, G. Gopakumar, M. T. Nguyen and A. Ceulemans, *Phys. Chem. Chem. Phys.*, 2011, **13**, 7524–7533.
18 M. Olguin, T. Baruah and R. R. Zope, *Chem. Phys. Lett.*, 2011, **514**, 66–69.
19 J. L. Li, Z. S. Hu and G. W. Yang, *Chem. Phys.*, 2012, **392**, 16–20.
20 H. T. Pham, L. V. Duong, N. M. Tam, M. P. Pham-Ho and M. T. Nguyen, *Chem. Phys. Lett.*, 2014, **608**, 295–302.

21 Q. Sun, M. Wang, Z. Li, A. J. Du and D. J. Searles, *J. Phys. Chem. C*, 2014, **118**, 2170–2177.
22 J. G. Wang, L. Ma, Y. H. Liang, M. L. Gao and G. H. Wang, *J. Theor. Comput. Chem.*, 2014, **13**, 1450050.
23 G. Garcia, M. Atilhan and S. Aparicio, *J. Phys. Chem. B*, 2015, **119**, 12455–12463.
24 R. X. He and X. C. Zeng, *Chem. Commun.*, 2015, **51**, 3185–3188.
25 L. J. Cheng, *J. Chem. Phys.*, 2012, **136**, 104301.
26 J. Lv, Y. C. Wang, L. Zhu and Y. M. Ma, *Nanoscale*, 2014, **6**, 11692–11696.
27 A. D. Becke, *Phys. Rev. A*, 1988, **38**, 3098–3100.
28 C. T. Lee, W. T. Yang and R. G. Parr, *Phys. Rev. B: Condens. Matter Mater. Phys.*, 1988, **37**, 785–789.
29 W. J. Stevens, H. Basch and M. Krauss, *J. Chem. Phys.*, 1984, **81**, 6026–6033.
30 S. Grimme, J. Antony, S. Ehrlich and H. Krieg, *J. Chem. Phys.*, 2010, **132**, 154104.
31 C. M. Breneman and K. B. Wiberg, *J. Comput. Chem.*, 1990, **11**, 361–373.
32 M. J. Frish, *et al.*, Gaussian, Inc, Wallingford CT, 2009.
33 V. V. Chaban and E. E. Fileti, *Phys. Chem. Chem. Phys.*, 2015, **17**, 15739–15745.
34 E. Fileti, G. Colherinhas and T. Malaspina, *Phys. Chem. Chem. Phys.*, 2014, **16**, 22823–22829.